de Ronde, C.E.J., Humphris, S.E., Höfig, T.W., and the Expedition 376 Scientists
Proceedings of the International Ocean Discovery Program Volume 376
publications.iodp.org

Data report: in situ elastic properties of hydrothermally altered volcanic rocks, IODP Expedition 376, Brothers volcano, Kermadec arc[1]

Ludmila Adam[2] and Cécile Massiot[3]

[1] Adam, L., and Massiot, C., 2022. Data report: in situ elastic properties of hydrothermally altered volcanic rocks, IODP Expedition 376, Brothers volcano, Kermadec arc. In de Ronde, C.E.J., Humphris, S.E., Höfig, T.W., and the Expedition 376 Scientists, Brothers Arc Flux. Proceedings of the International Ocean Discovery Program, 376: College Station, TX (International Ocean Discovery Program). https://doi.org/10.14379/iodp.proc.376.201.2022
[2] School of Environment, University of Auckland, New Zealand. **l.adam@auckland.ac.nz**
[3] GNS Science, New Zealand.

Contents

Keywords
International Ocean Discovery Program, IODP, *JOIDES Resolution*, Expedition 376, Brothers Arc Flux, Site U1527, Site U1528, Site U1530, *P*-wave velocity, *S*-wave velocity, porosity, effective pressure

Supplementary material

References (RIS)

MS 376-201
Received 15 December 2020
Accepted 24 April 2022
Published 15 August 2022

Abstract

Cores and downhole measurements recovered during International Ocean Discovery Program (IODP) Expedition 376 to Brothers volcano in the Kermadec arc provided unprecedented in situ data in an active submarine arc caldera with extensive hydrothermal alteration. Pressure (*P*)-wave velocities were measured on the R/V *JOIDES Resolution* at atmospheric pressures and saturated with seawater. To complement these shipboard measurements, seven new samples were selected representing various primary lithologic and alteration mineralogic compositions in the three deepest holes (U1527C, U1528D, and U1530A) for further shore-based laboratory testing. *P*- and shear (*S*)-wave velocities and porosity were measured on seven samples at atmospheric pressure and dry conditions. In addition, *P*- and *S*-wave velocities of two of these samples were measured under effective pressure dry and brine saturated. Such data aids in situ porosity, saturation, and pressure sensitivity elastic data interpretation from downhole measurements acquired in Hole U1530A. The clear waveforms obtained and overall similarities to measurements from the nearest shipboard samples ensure that the results are reliable at atmospheric pressures. All shore-based samples have higher porosity than shipboard samples. This difference could be explained by gas- versus water-connected porosity. The two saturated samples measured at effective pressures of the borehole sample depths show that *P*-wave speeds are 13%–20% higher than the ship atmospheric pressure measurements. The pressure dependence of wave speeds also enables the qualitative interpretation of pore shapes for these submarine, hydrothermally altered rocks.

1. Introduction

International Ocean Discovery Program (IODP) Expedition 376 drilled a series of holes at Brothers volcano in 2018 (**de Ronde et al.**, 2019a; de Ronde et al., 2019b). Brothers volcano is an active submarine caldera and one of 34 large volcanic complexes of the Kermadec arc (de Ronde et al., 2001, 2003). Volcanic rocks span a wide range in physical and hydraulic properties, the result of their varied lithologies and associated microstructures, vesicularity, fracturing (primary and subsequent faulting), alteration mineral assemblages, alteration intensity, and compaction as a consequence of sequential deposition of volcanic products (McPhie and Allen, 1992; Bartetzko et al., 2005; Wyering et al., 2014; Heap et al., 2017; Clarke et al., 2020; Durán et al., 2019; Kanakiya et al., 2021).

Elastic property measurements of core samples support interpretation of in situ porosity, saturation, and pressure sensitivity elastic data of both downhole sonic measurements as conducted in Hole U1530A during Expedition 376 (Massiot et al., 2022). It may assist in future time-to-depth

conversions of seismic reflection surveys to reveal the internal structure of Brothers volcano (**de Ronde et al.**, 2019a).

Shipboard physical properties measurements included *P*-wave velocity but not *S*-wave velocity. *P*-wave velocity analysis was conducted at atmospheric pressure and temperature. Shipboard measurements are reported in **de Ronde et al.** (2019a) and are available through the IODP laboratory information management system (LIMS) data portal (**https://web.iodp.tamu.edu/LORE**). Interpretations of shipboard core sample physical properties and downhole measurements for Holes U1530A and U1528D are summarized in Massiot et al. (2022). The acquisition of *S*-wave velocity data allows for the estimation of rock dynamic elastic moduli, aids converted-wave seismic interpretation, and can be used to quantitatively invert for pore shape. Measurements at atmospheric conditions are useful and rapid to obtain, but they do not directly reflect the in situ subseafloor conditions where the samples were collected.

This study aims to provide two types of measurements not acquired shipboard: (1) combined *P*- and *S*-wave velocities and porosity at atmospheric temperature and pressure in dry conditions and (2) *P*- and *S*-wave velocities on dry and water-saturated samples under effective pressure.

2. Materials

Seven core samples were analyzed in this study, representing a variety of primary rock textures and alteration mineral assemblages across the three main holes (U1527C, U1528D, and U1530A) at Brothers volcano (Table **T1**). Samples from Hole U1527C are matrix-supported, polymict tuff-breccia (Sections 14R-2 and 14R-3). Samples from Hole U1528D are clast-supported, polymict lapillistone (Section 17R-1); matrix-supported, polymict lapilli-tuff (Section 20R-1); and an altered volcanic rock part of a unit dominantly composed of volcaniclastic rocks (Section 42R-1). Samples from Hole U1530A are matrix-supported, monomict lapilli-tuff (Section 25R-1) and an altered volcanic rock showing overprinted volcanic textures (Section 50R-1). In this latter case, Massiot et al. (2022) proposed that the surrounding interval consists dominantly of altered lava flows. All samples are intensely hydrothermally altered. Alteration mineralogy for each sample is summarized in Table **T1**, based on shipboard visual core descriptions and X-ray diffraction measurements (**de Ronde et al.**, 2019a).

3. Methods

Shipboard *P*-wave velocity was measured on cube-shaped water-saturated samples using the *P*-wave caliper (PWC) of the *P*-wave gantry system (**de Ronde et al.**, 2019a). Cubes were vacuumed and saturated with seawater for 2 h at ambient pressure. Ultrasonic (500 kHz) *P*-wave waveforms were measured in three orthogonal directions on these saturated samples. Traveltimes are automatically picked by the IMS 10 velocity software in the PWC system and checked manually. The shipboard values reported in Table **T1** are the averaged *P*-wave velocities in the *x*-, *y*-, and *z*-directions, following standard IODP conventions. However, *S*-wave velocities were not acquired. Bulk dry density, grain density, and connected porosity were measured on the cube samples using the moisture and density apparatus that uses a dual-balance system (**de Ronde et al.**, 2019a). Some of these cube samples were subsequently used in thermal demagnetization experiments for paleomagnetism (**de Ronde et al.**, 2019a), which likely altered the samples' physical properties through exposure to temperatures as high as 600°C.

Shipboard samples could not be used in this study because of their shape and exposure to thermal impact. The shore-based high-pressure ultrasonic system used in this study requires cylindrically shaped samples ("CYL" in IODP sample naming convention). Measurements obtained from shore-based samples are compared to the results from the nearest shipboard samples (i.e., showing an offset of <50 cm; Table **T1**).

Table T1. Properties of samples measured in this study and the closest shipboard measurements, Holes U1527C, U1528D, and U1530A. **Download table in CSV format.**

In this study, the following tests were conducted:

- Porosity (nitrogen gas) and *P*- and *S*-wave velocities (V_P and V_S) were measured at atmospheric pressure in dry conditions on seven samples.
- *P*- and *S*-wave velocities were measured under pressure in dry and saltwater-saturated conditions for Samples CYL9673831 and CYL9674801, which are both from Hole U1530A.

Atmospheric condition porosity and wave speed data were acquired on dry samples with the nitrogen Vinci pycnometer and Olympus ultrasonic transducers (0.5 MHz central frequency), respectively.

P- and *S*-wave velocities measured at high pressure used an in-house built ultrasonic transducer system (one *P*-wave and two orthogonal *S*-waves; 1 MHz central frequency) at the University of Auckland (New Zealand), including capabilities of up to 68 MPa (10,000 psi) of confining pressures and 62 MPa (9,000 psi) of fluid pressure (Durán Quintero, 2018). A Teledyne Isco 65DM syringe pump controls the fluid pressures with independent pressure and fluid controls. A high-pressure transfer vessel allows the saturation of saline water (NaCl at 35 g/L) into the samples. Error bars were estimated to be about 30 m/s for *P*-waves and 60–100 m/s for *S*-waves.

The effective pressure of the depth from where these cores were extracted in the borehole is not fully known. That is because the fluid pressure is unknown. We infer that the fluid column does not influence the fluid pressure but rather the lithostatic load. The water column (~1.6 km) and the weight of the rocks act as the lithostatic pressure. The fluid pressure was assumed to be that of when the rocks erupted (i.e., the water column pressure), referring to 15 MPa. Effective pressure is the difference between the lithostatic and fluid pressures. Therefore, for these rocks, the effective pressure is 3.1 and 1.6 MPa for Samples CYL9674801 (376-U1530A-50R-1, 69–71 cm; 242.59–242.61 meters below seafloor [mbsf]) and CYL9673831 (25R-1 41–43 cm; 122.31–122.33 mbsf), respectively.

The measurements under effective pressure were conducted per the following procedure:

1. Measurements of samples in dry conditions were subjected to increasing and then decreasing pressure. The recorded (main) cycle referred to the instrument run with decreasing pressure to reduce hysteresis. Wave speeds were recorded at regular pressure increments.
2. Samples were saturated for 2–4 days with saltwater (NaCl at 35 g/L) at 2 MPa fluid pressure and 4.1 MPa (600 psi) confining pressure. Fluid pressure was kept constant at 2 MPa for all the saturated experiments.
3. The first pressure cycle on saturated samples was performed at low effective pressures to avoid permanent sample deformation. The maximum effective pressures were 1.6 MPa (240 psi) for Sample CYL9673831 and 4.5 MPa (650 psi) for Sample CYL9674801, which enabled measurement of in-place sample depths: 1.6 MPa (232 psi) for Sample CYL9673831 and 3.1 MPa (447 psi) for Sample CYL9674801.
4. The second water-saturated cycle was performed at higher effective pressure: up to 31 MPa (4500 psi) for Sample CYL9674801 and 13.8 MPa (2000 psi) for Sample CYL9673831. This cycle was done after low effective pressures to guarantee that samples were not permanently deformed during the third part of the test.

4. Results

The results of shore-based measurements are presented in Table **T1** and TABLE in **Supplementary material** alongside shipboard measurements of the closest samples. Shipboard and shore-based samples have similar porosity (absolute difference < 5%), and most *P*-wave velocity differences are within 250 m/s (Figure **F1**; Table **T1**). Samples from Hole U1527C are 1.6 m apart in the stratigraphic succession and are part of the same petrophysical subunit (2b) and alteration subtype (IIa) (Massiot et al., 2022), thus, their wave speeds and porosity are similar. Samples from other boreholes do not belong to the petrophysical unit or alteration type and were not sampled within

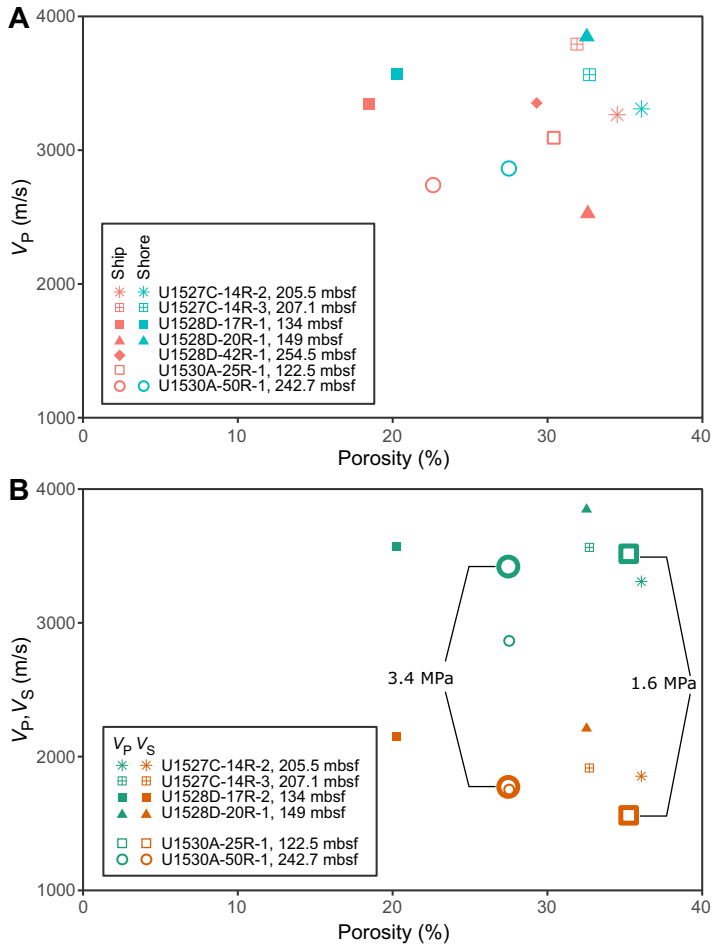

Figure F1. Wave velocities as a function of porosity. A. V_P, shipboard and nearest shore-based samples (this report). B. V_P and V_S, shore-based samples. Large symbols are measurements at effective pressure representative of core downhole depth (1.6 MPa for 376-U1530A-25R-1, 41–43 cm; 3.4 MPa for 50R-1, 69–71 cm). Shipboard data from de Ronde et al. (2019a).

a short stratigraphic distance. Therefore, because samples are few in number, we cannot propose any generalization or statistical trends on velocity versus porosity data presented here. Shipboard samples were measured water saturated, whereas present samples at atmospheric conditions were dry. It is unclear why shipboard seawater-saturated V_P are similar to shore-based dry V_P.

Nitrogen porosity of shore-based samples is consistently slightly higher than seawater-saturated connected porosity from shipboard samples. This is expected because nitrogen can reach smaller pores than water because of reduced capillary forces, resulting in a higher estimate of connected porosity.

One doublet of samples shows large differences in porosity and wave speed between shore-based and shipboard samples. Sample 376-U1528D-20R-1, 114–117 cm, has higher grain density (3.4 g/cm^3) and *P*-wave velocity (3848 m/s) than the nearest shipboard sample (20R-1, 100–102 cm; 2.66 g/cm^3 and 2526 m/s, respectively). This core section consists of a matrix-supported, polymict lapilli-tuff, meaning the matrix supports clasts of various sizes (**de Ronde et al.**, 2019a) possibly resulting in sample heterogeneity. Figure **F2** shows line section images of the core section from which the samples were extracted. In this section (20R-1), visual core description revealed a high sulfur abundance, with native sulfur infilling vugs throughout the matrix as well as disseminated pyrite (**de Ronde et al.**, 2019a). The difference between the two samples only 20 cm apart along the core section is thus likely due to a variable pyrite content and sulfur-filled vugs, which can result in higher rock density and velocity.

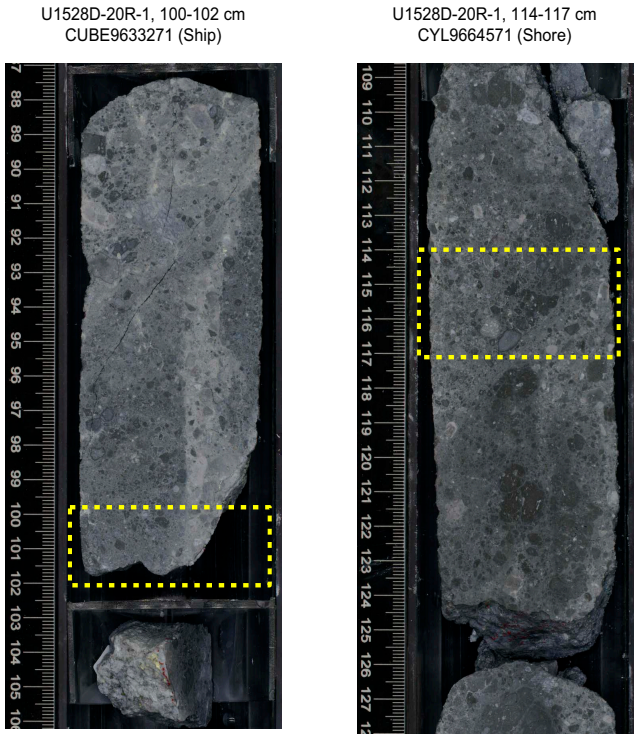

Figure F2. Core section images (376-U1528D-20R-1, 87–106 cm, and 107–127 cm), highlighting location where Samples CUBE9633271 and CYL9664571 were extracted. Section was described in de Ronde et al. (2019a) as matrix-supported, polymict lapilli-tuff. Section has pervasive alteration and is dominated by 1–3 mm sized light gray to dark gray clasts that are highly silicified in a fine network of clay- and silica-dominated matrix. Native sulfur infills vugs throughout the matrix. Pyrite is disseminated and seems to be more concentrated in clasts. Photos are in color.

High-quality waveforms and classic relationships yield good confidence in the results performed in this study. Figure **F3** displays ultrasonic waveforms for the measurements under effective pressure. Traveltimes were picked and converted to wave speed for all saturation conditions and effective pressures (Figure **F4**). First, V_P in saturated condition is greater than V_P in dry condition and V_S in saturated condition is lower than V_S in dry condition. Second, dry wave speeds under pressure are higher than measurements at atmospheric pressure. Both samples show a significant increase in wave speeds after applying only a few megapascals of effective pressure when compared to the atmospheric velocity data.

Although Sample 376-U1530A-25R-1, 41–43 cm, has higher porosity than Sample 50R-1, 69–71 cm, the lower pressure dependence of V_P and V_S (Figure **F4**) suggests that Sample 25R-1, 41–43 cm, has higher aspect ratio and stiffer pores than Sample 50R-1, 69–71 cm, with the latter having more low-aspect ratio pores (i.e., microfractures). This result is consistent with other physical properties (Massiot et al., 2022).

For both samples, V_P on seawater-saturated samples after the high-pressure cycle (Step 4 above) is lower than the first low-pressure cycle and the dry pressure cycle. This directly indicates that the sample underwent permanent deformation during the second, high-pressure cycle. Such experiments show that care needs to be taken when performing velocity measurements on core material at high confining pressures. When comparing core physical property data to downhole measurements, measurements that correspond to the core-downhole pressure conditions first need to be performed before attempting any experiments at higher effective pressures.

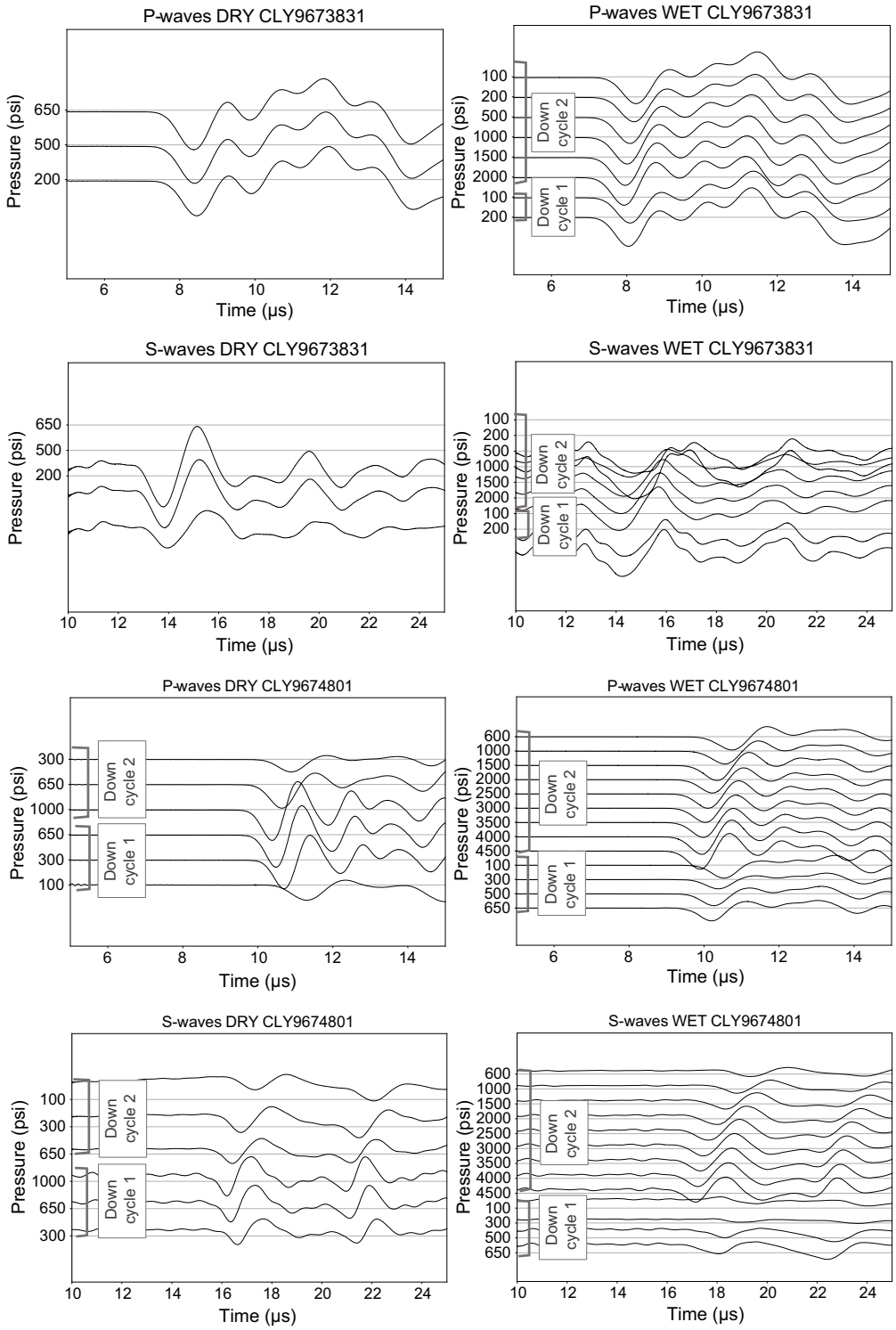

Figure F3. Ultrasonic waveforms for measurements under effective pressure for dry and water-saturated (WET) samples, Hole U1530A.

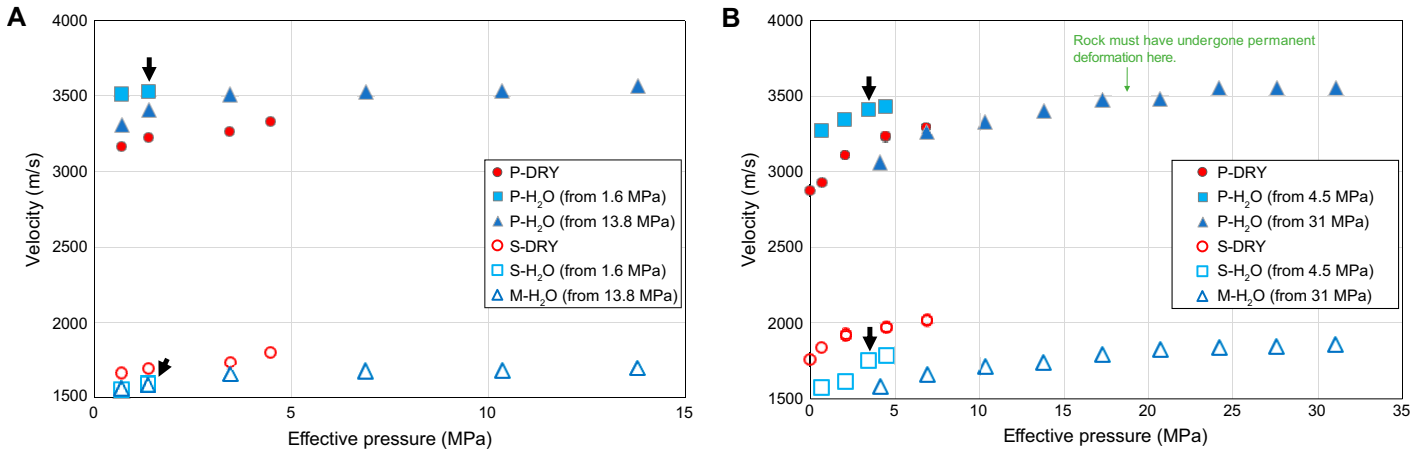

Figure F4. V_P and V_S as a function of effective pressure, Hole U1530A. Fluid pressure is constant at 2 MPa for saturated samples. A. Sample CYL9673831 (25R-1, 41–43 cm; 122.3 mbsf). B. Sample CYL9674801 (50R-1, 69–71 cm; 242.6 mbsf). Black arrows = effective pressure representative of sample depth.

5. Acknowledgments

This research used samples and data provided by the International Ocean Discovery Program (IODP). We thank the IODP technical staff and the R/V *JOIDES Resolution* crew for their invaluable support and perseverance during a challenging expedition. Support for C. Massiot by the New Zealand government via the Te Riu a Māui/Understanding Zealandia research program led by GNS Science is acknowledged.

References

Adam, L., and Massiot, C., 2022. Supplementary material, **https://doi.org/10.14379/iodp.proc.376.201supp.2022**. In Adam, L., and Massiot, C., Data report: in situ elastic properties of hydrothermally altered volcanic rocks, IODP Expedition 376, Brothers volcano, Kermadec arc. In de Ronde, C.E.J., Humphris, S.E., Höfig, T.W., and the Expedition 376 Scientists, Brothers Arc Flux. Proceedings of the International Ocean Discovery Program, 376: College Station, TX (International Ocean Discovery Program).

Bartetzko, A., Delius, H., and Pechnig, R., 2005. Effect of compositional and structural variations on log responses of igneous and metamorphic rocks. I: Mafic rocks. In Harvey, P.K., Brewer, T.S., Pezard, P.A., and Petrov, V.A. (Eds.), Petrophysical Properties of Crystalline Rocks. Geological Society Special Publication, 240:255–278. **https://doi.org/10.1144/GSL.SP.2005.240.01.19**

Christaras, B., Auger, F., and Mosse, E., 1994. Determination of the moduli of elasticity of rocks. Comparison of the ultrasonic velocity and mechanical resonance frequency methods with direct static methods. Materials and Structures, 27(4):222–228. **https://doi.org/10.1007/BF02473036**

Clarke, J., Adam, L., van Wijk, K., and Sarout, J., 2020. The influence of fluid type on elastic wave velocity and attenuation in volcanic rocks. Journal of Volcanology and Geothermal Research, 403:107004. **https://doi.org/10.1016/j.jvolgeores.2020.107004**

de Ronde, C.E., Faure, K., Bray, C.J., Chappell, D.A., and Wright, I.C., 2003. Hydrothermal fluids associated with seafloor mineralization at two southern Kermadec arc volcanoes, offshore New Zealand. Mineralium Deposita, 38(2):217–233. **https://doi.org/10.1007/s00126-002-0305-4**

de Ronde, C.E.J., Baker, E.T., Massoth, G.J., Lupton, J.E., Wright, I.C., Feely, R.A., and Greene, R.R., 2001. Intra-oceanic subduction-related hydrothermal venting, Kermadec volcanic arc, New Zealand. Earth and Planetary Science Letters, 193(3–4):359–369. **https://doi.org/10.1016/S0012-821X(01)00534-9**

de Ronde, C.E.J., Humphris, S.E., Höfig, T.W., Brandl, P.A., Cai, L., Cai, Y., Caratori Tontini, F., Deans, J.R., Farough, A., Jamieson, J.W., Kolandaivelu, K.P., Kutovaya, A., Labonté, J.M., Martin, A.J., Massiot, C., McDermott, J.M., McIntosh, I.M., Nozaki, T., Pellizari, V.H., Reyes, A.G., Roberts, S., Rouxel, O., Schlicht, L.E.M., Seo, J.H., Straub, S.M., Strehlow, K., Takai, K., Tanner, D., Tepley III, F.J., and Zhang, C., 2019a. Expedition 376 summary. In de Ronde, C.E.J., Humphris, S.E., Höfig, T.W., and the Expedition 376 Scientists, Brothers Arc Flux. Proceedings of the International Ocean Discovery Program, 376: College Station, TX (International Ocean Discovery Program). **https://doi.org/10.14379/iodp.proc.376.101.2019**

de Ronde, C.E.J., Humphris, S.E., Höfig, T.W., Reyes, A.G., and the IODP Expedition 376 Scientists, 2019b. Critical role of caldera collapse in the formation of seafloor mineralization: the case of Brothers volcano. Geology, 47(8):762–766. **https://doi.org/10.1130/G46047.1**

Durán, E.L., Adam, L., Wallis, I.C., and Barnhoorn, A., 2019. Mineral alteration and fracture influence on the elastic properties of volcaniclastic rocks. Journal of Geophysical Research: Solid Earth, 124(5):4576–4600. **https://doi.org/10.1029/2018JB016617**

Durán Quintero, E., 2018. Fracture and rock alteration characterization from geophysical well logs and core: Ngatamariki geothermal field [PhD dissertation]. The University of Auckland, Auckland, New Zealand. **http://hdl.handle.net/2292/41228**

Heap, M.J., Kennedy, B.M., Farquharson, J.I., Ashworth, J., Mayer, K., Letham-Brake, M., Reuschlé, T., Gilg, H.A., Scheu, B., Lavallée, Y., Siratovich, P., Cole, J., Jolly, A.D., Baud, P., and Dingwell, D.B., 2017. A multidisciplinary approach to quantify the permeability of the Whakaari/White Island volcanic hydrothermal system (Taupo Volcanic Zone, New Zealand). Journal of Volcanology and Geothermal Research, 332:88–108. **https://doi.org/10.1016/j.jvolgeores.2016.12.004**

Kanakiya, S., Adam, L., Rowe, M.C., Lindsay, J.M., and Esteban, L., 2021. The role of tuffs in sealing volcanic conduits. Geophysical Research Letters, 48(20):e2021GL095175. **https://doi.org/10.1029/2021GL095175**

Massiot, C., McIntosh, I., Deans, J., Milicich, S.D., Caratori Tontini, F., de Ronde, C.E.J., Adam, L., Kolandaivelu, K., and Guerin, G., 2022. Petrophysical facies and inferences on permeability at Brothers Volcano, Kermadec arc, using downhole images and petrophysical data. Economic Geology. **https://doi.org/10.5382/econgeo.4897**

McPhie, J., and Allen, R.L., 1992. Facies architecture of mineralized submarine volcanic sequences; Cambrian Mount Read Volcanics, western Tasmania. Economic Geology, 87(3):587–596. **https://doi.org/10.2113/gsecongeo.87.3.587**

Wyering, L.D., Villeneuve, M.C., Wallis, I.C., Siratovich, P.A., Kennedy, B.M., Gravley, D.M., and Cant, J.L., 2014. Mechanical and physical properties of hydrothermally altered rocks, Taupo Volcanic Zone, New Zealand. Journal of Volcanology and Geothermal Research, 288:76–93. **https://doi.org/10.1016/j.jvolgeores.2014.10.008**